Electronic Supplementary Material (ESI) for Journal of Materials Chemistry A.

Prediction of higher thermoelectric performance in BiCuSeO by weakening electron-polar optical phonon scattering

T. Zhao,* Q. D. Gibson, L. M. Daniels, B. Slater and F. Corà*

*Corresponding authors. Email: f.cora@ucl.ac.uk, tianqi.zhao@ucl.ac.uk

Analysis for the choice of DFT functionals

Here we analyse how the choice of DFT functionals affect structural and electronic properties of BiCuSeO, in order to 1) verify that the chosen functionals are accurate in reproducing the known properties of BiCuSeO; 2) show how big a variation is introduced when a different functional is chosen.

In terms of accuracy, we have divided the calculated values into structural (equilibrium lattice parameters, elastic constants and phonon frequencies) and electronic (band gap, dispersion of the bands in reciprocal space) properties. The former is calculated using the dispersion-corrected functional optB86b-vdW. Several comparisons are provided that reinforce the accuracy of our settings: equilibrium lattice parameters show very good match to experimental structure determination (Table S1), and phonon calculations yield excellent agreement to measured frequencies (Table S2). Dielectric constants and Born charges are shown in Table S3. Independent elastic constants are shown in Table S4. The optB86b-vdW results compare well with literature.

Electronic properties require orbital-dependent terms (hybrid exchange or DFT+U) for the localised Cu-3*d* states, and spin-orbit coupling for the Bi-6*sp*. We have employed the PBE+U+SOC description that requires the lowest computational overhead to describe both terms simultaneously. The most relevant comparison in this case is with the measured value of the band gap. There is unfortunately no direct comparison with experiment for the band structure; we can however show that any level of theory of lower accuracy introduces appreciable changes to the PBE+U+SOC band dispersion, which invalidates its use. On the contrary, comparison of the PBE+U results with those from the hybrid exchange functional HSE06, which is in principle superior to PBE+U, are negligible. This links to the second issue, and an estimate of errors arising from the wrong settings.

The optimised lattice parameters with a selection of functionals is given in Table S1; as soon as dispersion is not included, the interlayer separation (***c*** direction) increases by 0.1-0.2Å and in turn this causes significant deviations in both phonon frequencies (Table S2, Fig. S1) and electronic polarizabilities (Table S3). On the other hand, the optimised lattice parameters show minor difference between PBE, PBE+U, PBE+SOC, and PBE+U+SOC, indicating the inclusion of SOC and orbital dependent parameters has a minimal effect on the lattice parameters.

Comparisons of band structures calculated with different functionals are provided in Fig. S2-S6. Firstly, the comparison of band structure calculated by using optB86b-vdW and PBE (Fig. S2 and S3) shows that the van der Waals interaction and the transit of exchange functional from optB86b to PBE have negligible effect on electronic states at band edges. Secondly, addition of SOC, either in PBE, PBE+U, or HSE06 (Fig. S3-S5), is critical because it modifies the bands at the very top of the VB and bottom of the CB in an appreciable way. In particular, SOC resolves the degeneracy of bands at the Z point of reciprocal space; instead of flat bands originating from Z in the solution without SOC, the SOC bands have significant dispersion and thus yield significantly different transport properties. Thirdly, we note that the inclusion of orbital dependent terms (hybrid exchange or DFT+U) is also indeed critical to open a band gap in the material. The GGA+SOC solution has no band gap and should thus be discarded. In contrast HSE06+SOC (hybrid exchange) and PBE+U+SOC give superimposable band structure (Fig. S6), and it is clear that the cheaper PBE+U+SOC formulation can be used without loss of accuracy.

Table S1. Comparison of calculated lattice parameter of BiCuSeO under various functionals with experimental results.

		a (Å)	***c*** (Å)
Experiment[1]		3.930	8.927
Functionals	optB86b-vdW	3.926	8.957
	PBE	3.952	9.076
	PBE+U	3.957	9.075
	PBE+SOC	3.957	9.108
	PBE+U+SOC	3.961	9.103

Table S2. Frequencies of polar optic phonon mode of BiCuSeO at Γ in cm^{-1}

PO phonon Modes	This work		Literature[2]	Experiment[3]
	PBE+U+SOC	optB86b-vdW		
E_u	52.7	56.2	61.2	
A_{2u}	82.4	91.4	89.4	92.0
E_u	124.9	135.9	142.7	
A_{2u}	165.8	175.2	178.6	
E_u	301.9	341.9	347.7	
A_{2u}	447.3	472.9	473.7	475.0

Table S3. Born effective charge and high frequency dielectric constant of BiCuSeO

		This work		Literature[2]
		PBE+U+SOC	optB86b-vdW	
Z^*_{Bi}	In plane	7.00	6.50	6.46
	Out of plane	6.00	5.94	5.93
Z^*_{O}	In plane	-4.62	-4.28	-4.28
	Out of plane	-4.40	-4.36	-4.42
Z^*_{Cu}	In plane	1.59	1.46	1.44
	Out of plane	1.22	1.09	1.06
Z^*_{Se}	In plane	-3.98	-3.67	-3.67
	Out of plane	-2.82	-2.67	-2.70
k_∞	In plane	26.38	17.61	18.01
	Out of plane	14.76	13.25	13.79

Table S4. Independent elastic constants C_{ii} of BiCuSeO in unit of GPa

	C_{11}	C_{12}	C_{13}	C_{33}	C_{44}	C_{66}
PBE+U+SOC (This work)	122.1	46.6	40.6	82.1	39.5	24.7
optB86b-vdW (This work)	155.1	71.9	67.5	103.7	45.3	32.3
PBEsol[4]	158.1	71.2	66.6	102.8	46.8	36.2

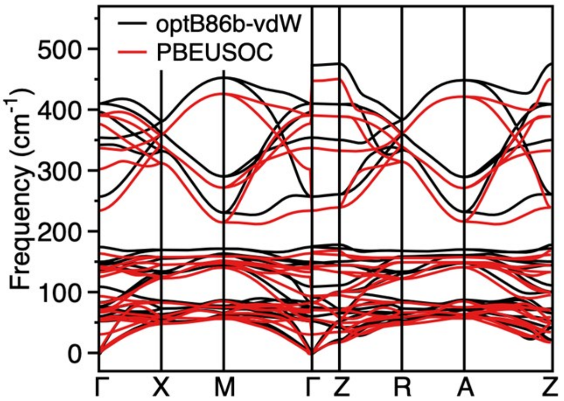

Fig. S1 The comparison of phonon band structure of BiCuSeO as calculated based on the optimized crystal structure under optB86b-vdW and PBE+U+SOC functional (including LO-TO splitting).

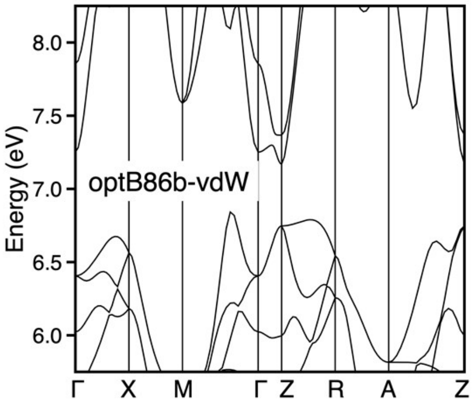

Fig. S2 Electronic band structure of BiCuSeO calculated by using optB86b-vdW functional.

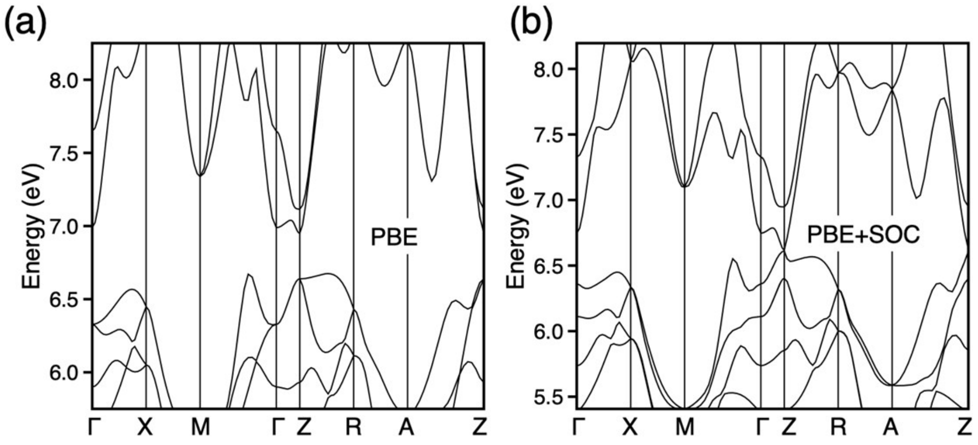

Fig. S3 Comparison of electronic band structure of BiCuSeO as calculated by using (a) PBE and (b) PBE+SOC functional.

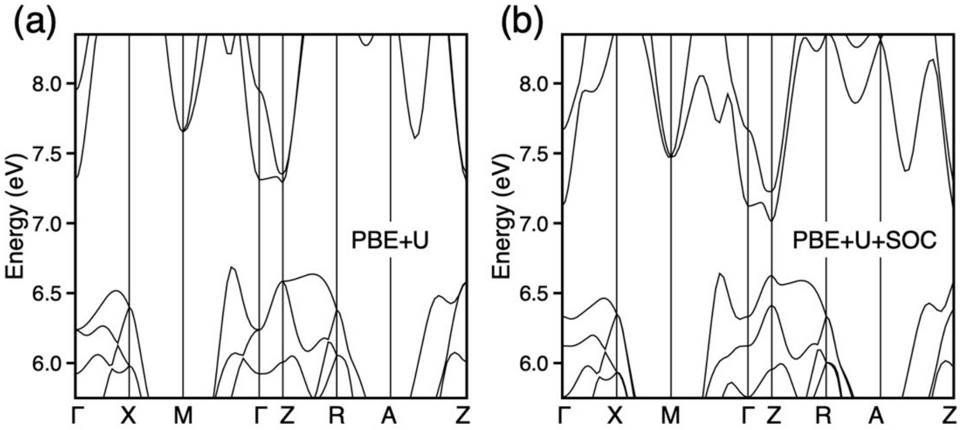

Fig. S4 Comparison of electronic band structure of BiCuSeO as calculated by using (a) PBE+U and (b) PBE+U+SOC functional.

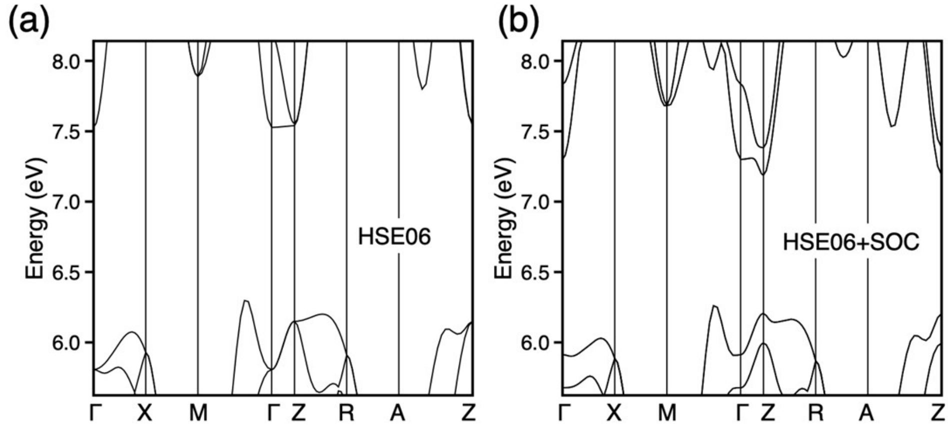

Fig. S5 Comparison of electronic band structure of BiCuSeO as calculated by using (a) HSE06 and (b) HSE06+SOC functional. The band gap are 1.23 and 0.93 eV for HSE06 and HSE06+SOC, respectively.

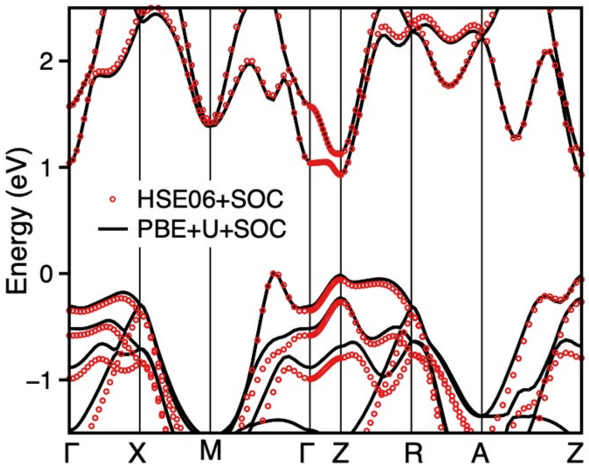

Fig. S6 The comparison of band structures of BiCuSeO as calculated from PBE+U+SOC functional with a rigid band shift of 0.57 eV on conduction bands and from HSE06+SOC functional. The band gap calculated with HSE06+SOC is 0.93 eV in this study. The energy of valence band maximum is set to zero.

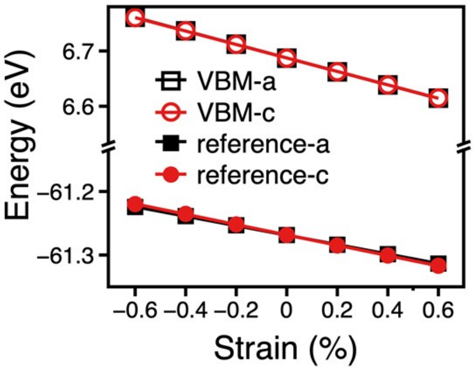

Fig. S7 Variation of VBM energy with strain in ***a*** and ***c*** direction under PBE+U functional. The reference energy of the Cu-3*p* core level used to obtain the deformation constants is also shown. The deformation potential in ***a*** and ***c*** direction are calculated to be 4.8 and 4.0 eV, respectively.

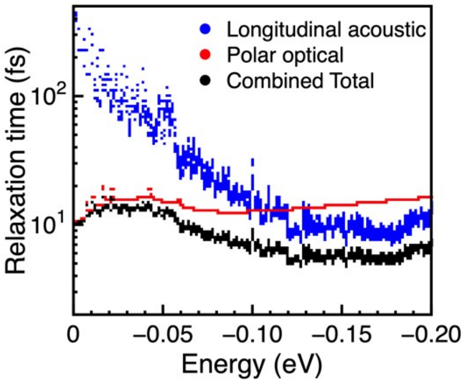

Fig. S8 Calculated relaxation time of holes at 300 K for different phonon scattering mechanisms versus energy at 300 K. The VBM is set to zero.

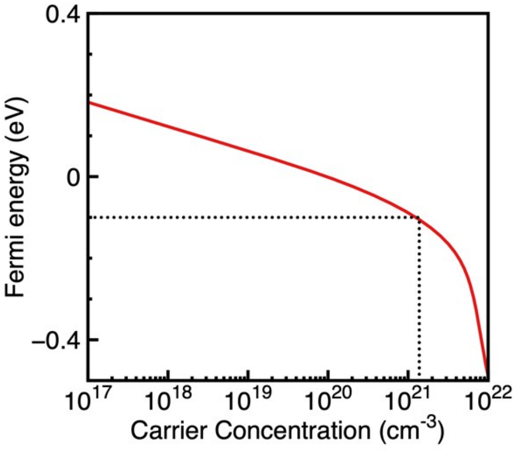

Fig. S9 Variation of carrier concentration with Fermi energy at 300 K in BiCuSeO. The energy zero is valence band maximum (VBM).

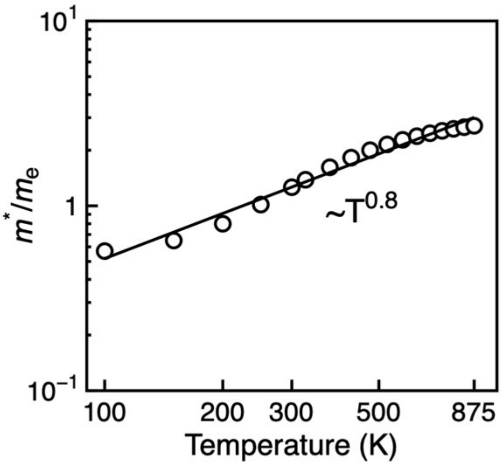

Fig. S10 Average effective mass versus temperature.

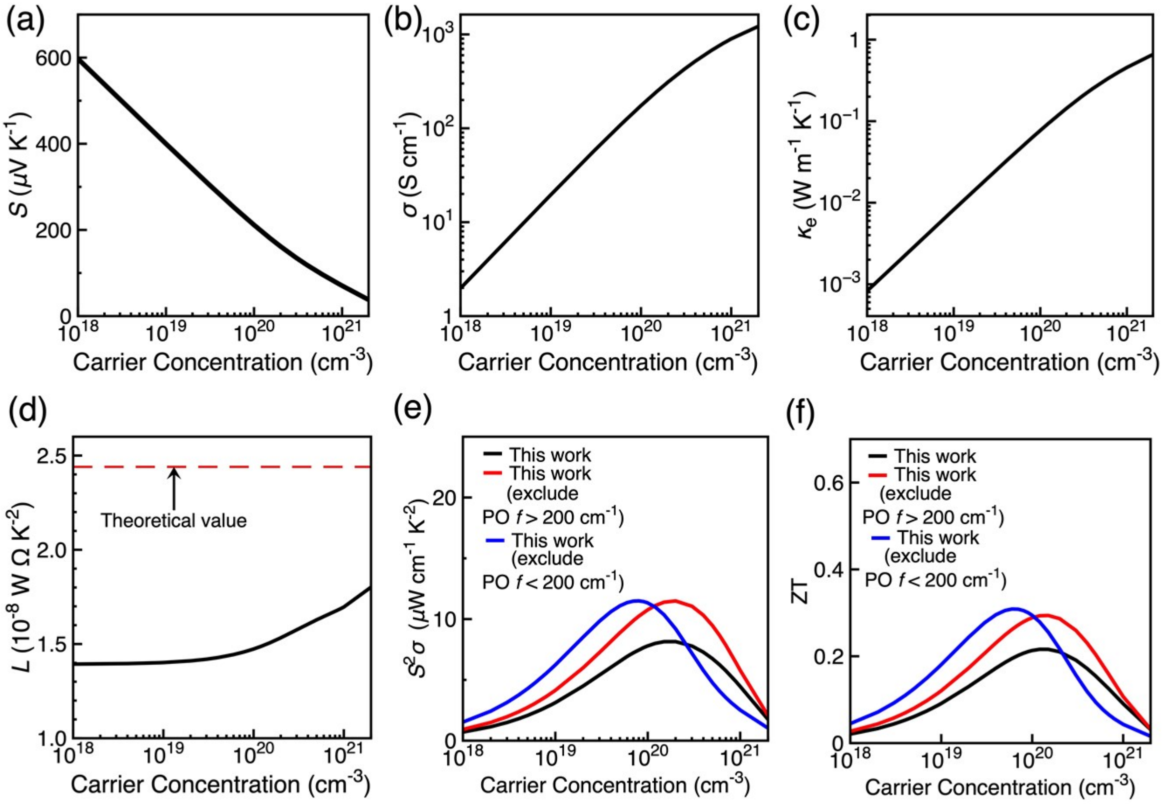

Fig. S11 Thermoelectric observables as a function of carrier concentration in the out-of-plane direction of BiCuSeO at 300 K: (a) Seebeck coefficient S, (b) electrical conductivity σ, (c) electrical thermal conductivity κ_e, (d) Lorenz number L, (e) thermoelectric power factor $S^2\sigma$, and (f) thermoelectric figure of merit ZT.

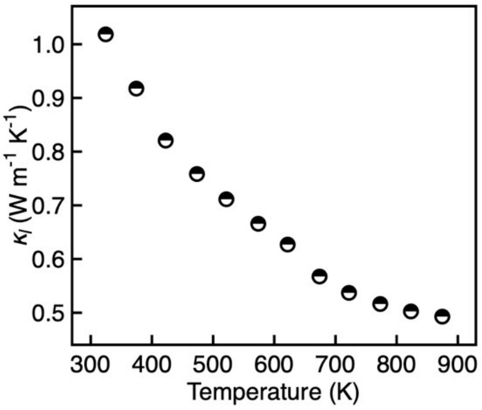

Fig. S12 Lattice thermal conductivity of BiCuSeO as reproduced from literature,[5] which is used to calculate thermoelectric figure of merit ZT of BiCuSeO in this work.

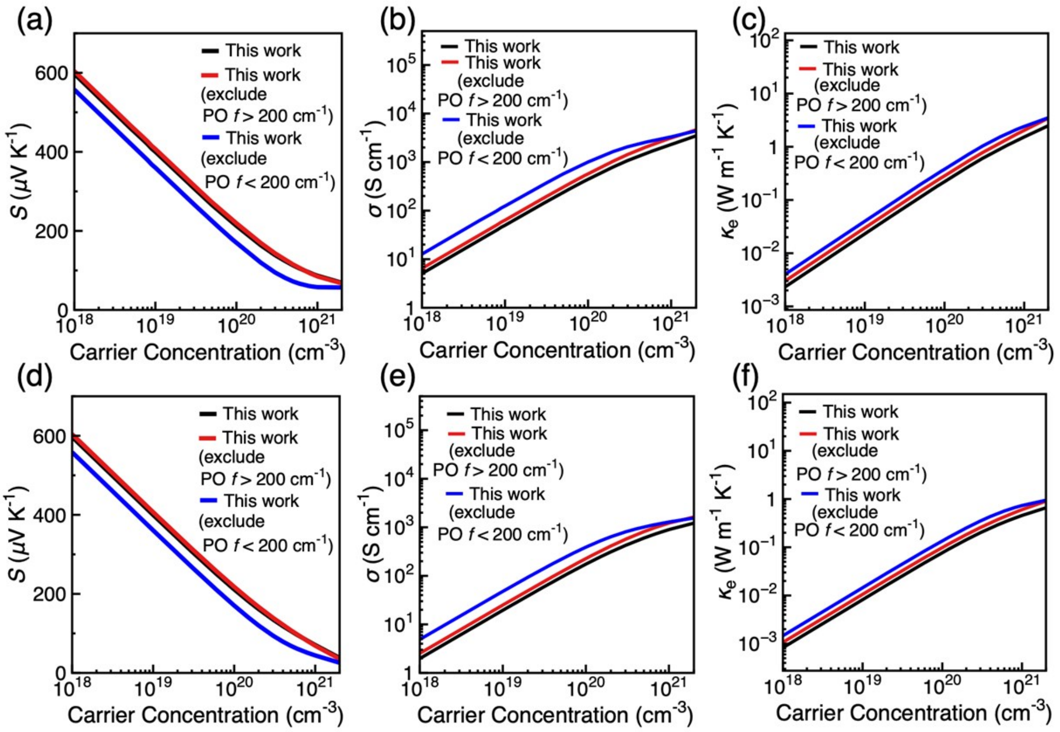

Fig. S13 The variation of thermoelectric charge transport properties with carrier concentration at 300 K. (a) Seebeck coefficient, (b) electrical conductivity, (c) electrical thermal conductivity in in-plane direction, and (d) Seebeck coefficient, (e) electrical conductivity, (f) electrical thermal conductivity in out-of-plane direction of BiCuSeO, as compared to that excluding PO phonon with frequency > 200 cm^{-1} and frequency < 200 cm^{-1}.

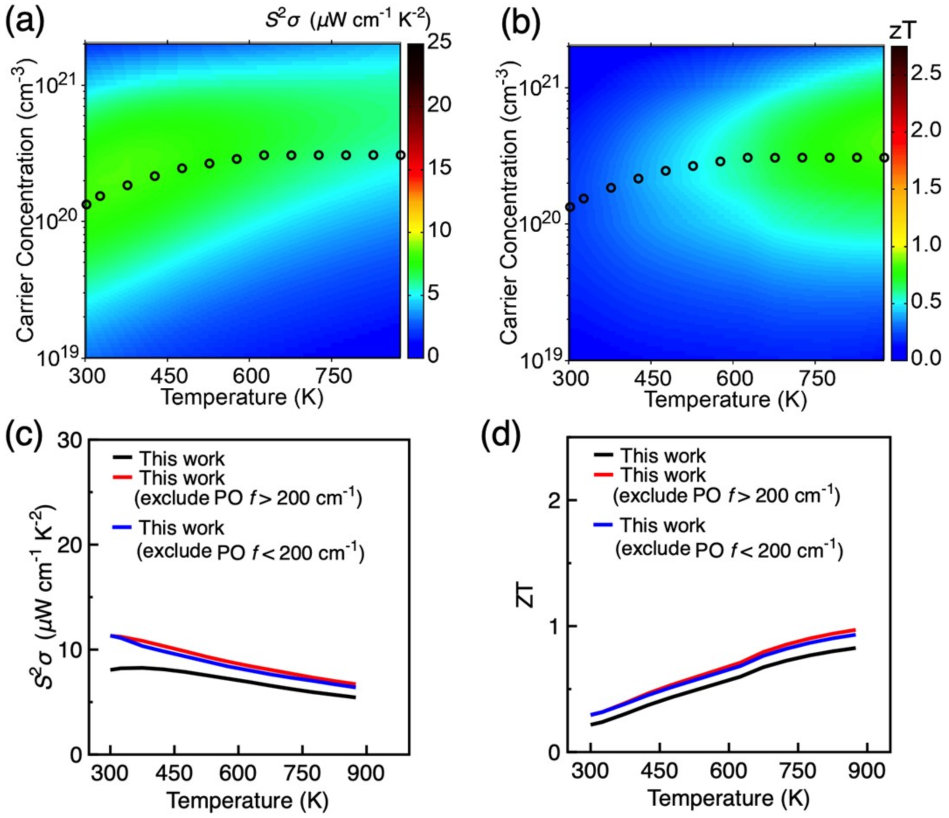

Fig. S14 (a) Variation of power factor $S^2\sigma$ and (b) thermoelectric figure of merit *ZT* with temperature and carrier concentration for p-type BiCuSeO. The circles denote the position of maximum *ZT* at each temperature. (c) Power factor and (d) optimal figure of merit *ZT* in the temperature range of 300-875 K. Data are shown for out-of-plane direction. Experimental values under various doping methods are shown for comparison.

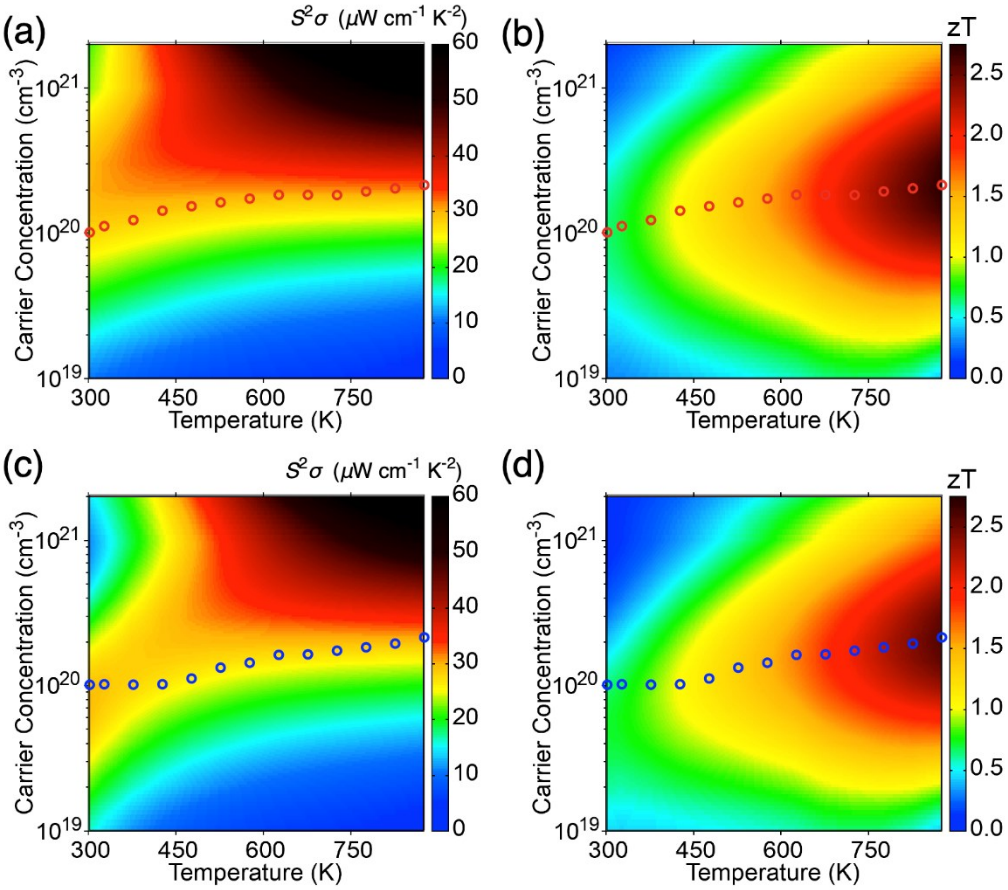

Fig. S15 The variation of in-plane (a) power factor and (b) ZT of BiCuSeO as a function of carrier concentration and temperature after excluding the scattering effects of PO phonon with frequency > 200 cm^{-1}. The variation of in-plane (c) power factor and (d) ZT of BiCuSeO as a function of carrier concentration and temperature after excluding the scattering effects of PO phonon with frequency < 200 cm^{-1}.

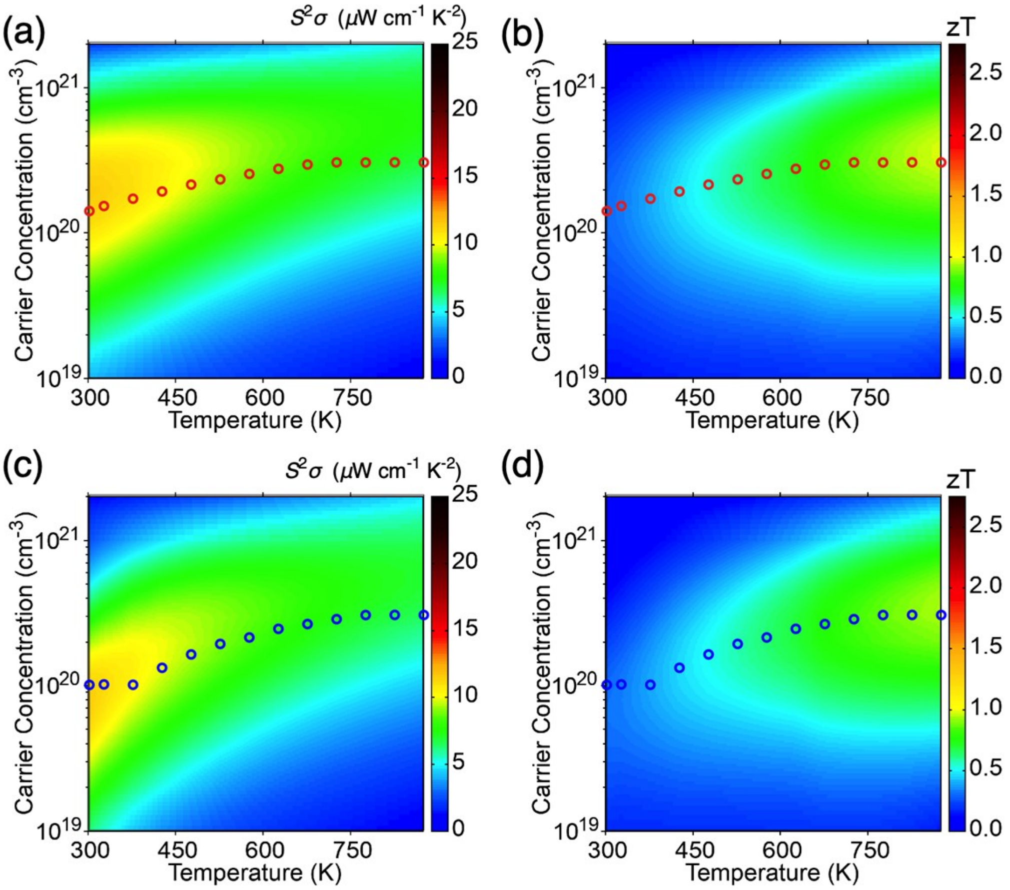

Fig. S16 The variation of out-of-plane (a) power factor and (b) ZT of BiCuSeO as a function of carrier concentration and temperature after excluding the scattering effects of PO phonon with frequency > 200 cm^{-1}. The variation of out-of-plane (c) power factor and (d) ZT of BiCuSeO as a function of carrier concentration and temperature after excluding the scattering effects of PO phonon with frequency < 200 cm^{-1}.

Reference:

1 L. D. Zhao, D. Berardan, Y. L. Pei, C. Byl, L. Pinsard-Gaudart and N. Dragoe, *Appl. Phys. Lett.*, 2010, **97**, 092118.

2 S. K. Saha, *Phys. Rev. B*, 2015, **92**, 041202(R).

3 P. S. Berdonosov, A. M. Kusainova, L. N. Kholodkovskaya, V. A. Dolgikh, L. G. Akselrud and B. A. Popovkin, *J. Solid State Chem.*, 1995, **118**, 74-77.

4 H. S. Ji, A. Togo, M. Kaviany, I. Tanaka and J. H. Shim, *Phys. Rev. B*, 2016, **94**, 115203.

5 G.-K. Ren, J.-l. Lan, S. Butt, K. J. Ventura, Y.-H. Lin and C.-W. Nan, *RSC Adv.*, 2015, **5**, 69878-69885.